Global Gyrokinetic Simulation of Linear Micro-Instability Using Parameters Referring to HL-2A Plasma with Ion Transport Barrier*)

Zhihao QIN, Kenji IMADERA, Jiquan LI[1)] and Yasuaki KISHIMOTO

Graduate School of Energy Science, Kyoto University, Uji, Kyoto 611-0011, Japan
[1)]*Southwestern Institute of Physics, Chengdu 610041, China*

(Received 3 January 2018 / Accepted 24 May 2018)

We study linear micro-instabilities using parameters referring to HL-2A plasma with ion Internal Transport Barrier (ITB) by means of the global toroidal gyrokinetic code GKNET including kinetic electron dynamics. It is found that a type of drift mode, which real frequency is low and changes the sign from electron diamagnetic direction to that of ion continuously as the poloidal wavenumber increases, dominates plasmas with peaked density profile while with relatively flat ion/electron temperature profiles. The instability is found to be sensitive to the perpendicular electron temperature $T_{e\perp}$, similar to the standard trapped electron mode, which is consistent with the observation of ion-ITB collapse after ECRH in the HL-2A experiment.

Keywords: gyrokinetic simulation, ITG mode, TEM, density gradient driven TEM, ITB

DOI: 10.1585/pfr.13.3403083

1. Introduction

Internal Transport Barrier (ITB), which acts as the shielding layer of particle and heat transport by suppressing turbulence, is a key to achieving high-performance plasmas. In recent HL-2A experiments [1], an ion-ITB is found to be formed just after the onset of co-NBI in the almost flat q-profile region. Recently, in our flux-driven Ion Temperature Gradient (ITG) driven turbulence simulations using GKNET with external momentum injection, we found that the mean radial electric field induced by a co-toroidal rotation through the radial force balance plays an important role in sustaining ITB in the plasma with flat q-profile [2], which is consistent with the HL-2A experiment. On the other hand, it is found that the ITB is collapsed after ECRH in the HL-2A experiment [1]. This indicates that Trapped Electron Mode (TEM) plays an important role, while the detailed mechanism has not been studied.

In order to understand which mode is responsible for the onset and collapse of the ion-ITB in HL-2A plasma, we perform a series of linear global ITG/TEM simulations by utilizing GKNET [3] which is an electrostatic 5D global Gyro-Kinetic (GK) code consisting of GK-Vlasov equation and that of GK-quasi-neutrality condition with kinetic electrons. Specifically, we investigate the linear ITG mode and TEM instability with the different ratio between parallel and perpendicular electron temperature $T_{e\perp}/T_{e\parallel}$ on to understand the effect of ECRH.

Here, in Sec. 2, we describe the model of the GKNET. In Sec. 3, linear analyses of dominant micro-instabilities using parameters referring to HL-2A plasma are presented. The impact of the ratio $T_{e\perp}/T_{e\parallel}$ on them is also discussed. Finally, a summary and future plan are given in Sec. 4.

2. Physical Model of GKNET

GK equations are derived in the 5D gyro-center coordinate system $(\boldsymbol{R}, \mu, v_\parallel)$ for species s, where $\boldsymbol{R}$ denotes the position of the guiding center, $\mu = m_s v_\perp^2/(2B)$ the magnetic moment, $v_\parallel$ the parallel velocity. The GK Vlasov equation is used to describe the evolution of gyro-center distribution function f_s as:

$$\frac{\mathrm{d}f_s}{\mathrm{d}t} \equiv \frac{\partial f_s}{\partial t} + \{f_s, H_s\} = \frac{\partial f_s}{\partial t} + \{\boldsymbol{R}, H_s\}\frac{\partial f_s}{\partial \boldsymbol{R}} + \{v_\parallel, H_s\} = 0, \quad (1)$$

where $H_s = m_s v_\parallel^2/2 + \mu B + e_s\langle\phi\rangle_\alpha$ is the gyro-center Hamiltonian [4]. The two Poisson brackets are de?ned as:

$$\{\boldsymbol{R}, H_s\} = \dot{\boldsymbol{R}} = v_\parallel \boldsymbol{b} + \frac{c}{e_s B_\parallel^*}\boldsymbol{b} \times (e_s\nabla\langle\phi\rangle_\alpha + m_s v_\parallel^2 \boldsymbol{b}\cdot\nabla\boldsymbol{b} + \mu\nabla B), \quad (2)$$

$$\{v_\parallel, H_s\} = \dot{v}_\parallel = -\frac{\boldsymbol{B}^*}{m_s B_\parallel^*}\cdot(e_s\nabla\langle\phi\rangle_\alpha + \mu\nabla B), \quad (3)$$

with m_s and e_s the mass and charge of the considered species and $\boldsymbol{B} = B\boldsymbol{b}$ denotes the magnetic field with the unit vector $\boldsymbol{b}$, $B_\parallel^* = \boldsymbol{B}^*\cdot\boldsymbol{b}$ is the parallel component of $\boldsymbol{B}^* = \boldsymbol{B} + (Bv_\parallel/\Omega_s)\nabla\times\boldsymbol{b}$ with gyro-frequency $\Omega_s = e_s B/m_s$. $\langle\phi\rangle_\alpha$ refers to the gyro-averaged electrostatic potential as:

$$\langle\phi\rangle_\alpha \equiv \frac{1}{2\pi}\oint_0^{2\pi}\phi(\boldsymbol{R}+\boldsymbol{\rho})\mathrm{d}\alpha. \quad (4)$$

author's e-mail: qin.zhihao.87m@st.kyoto-u.ac.jp, lijq@swip.ac.cn

*) This article is based on the presentation at the 26th International Toki Conference (ITC26).

ϕ is given by the GK quasi-neutrality condition

$$\left\{e_i[1-\Gamma_0(k_\perp^2\rho_{ti}^2)]\frac{T_e}{T_i}+e_e[1-\Gamma_0(k_\perp^2\rho_{te}^2)]\right\}\frac{\phi}{T_e} = \iint[e_i\delta f_i J_0(k_\perp\rho_i)+e_e\delta f_e J_0(k_\perp\rho_e)]m_s^2 B_\parallel^* \mathrm{d}v_\parallel \mathrm{d}\mu, \tag{5}$$

where $n_i = n_e \equiv n_0$ is assumed. Here $\rho_{ts} = m_s v_{ts}/e_s B$, so that ρ_i and ρ_e are the ion and electron gyro-radius, J_0 the Bessel function of the zeroth order, $\Gamma_0(k_\perp^2\rho_{ts}^2) = I_0(k_\perp^2\rho_{ts}^2)\exp(-k_\perp^2\rho_{ts}^2)$, I_0 is 0th-order modified Bessel function. The first and second terms in the right hand side are perturbed ion and electron densities, respectively. The non-adiabatic electron effect is included in the second term, which is essential to treat trapped electron dynamics.

The equilibrium distribution function is given by

$$F_s = n\sqrt{\frac{m_s^3}{2\pi(\Lambda_s^2 T_{s\parallel}^3)}}\exp\left[-\left(\frac{v_\parallel^2}{2}+\frac{\mu B}{\Lambda_s}\right)\frac{m_s}{T_{s\parallel}}\right], \tag{6}$$

where $\Lambda_s = T_{s\perp}/T_{s\parallel}$ is the ratio of perpendicular temperature to parallel temperature. In Sec. 3.3, Λ_e is changed to study the effect of ECRH, while the ratio for ion species is fixed as $\Lambda_i \equiv 1$. The trapped electron density is described as a function of Λ_e as

$$n_{e,trap} = \int_{-\infty}^{\infty}\int_{\mu_B}^{\infty} F_e m_s^2 B_\parallel^* \mathrm{d}v_\parallel \mathrm{d}\mu = n_0\sqrt{\frac{\Lambda_e\epsilon_0(1+\cos\theta)}{1+\epsilon_0(\Lambda_e-1)+\epsilon_0(\Lambda_e+1)\cos\theta-\epsilon_0^2\cos\theta}}, \tag{7}$$

where $\epsilon_0 = r/R_0$ is the inverse aspect ratio and $\mu_B = v_\parallel(R_0 - r)(R_0 + r\cos\theta)/[2R_0 r(1+\cos\theta)]$. Note that electrons are treated full-kinetically in the simulation.

3. Linear Analyses of Micro-Instabilities Referring to HL-2A Plasma

In this section, we perform linear analyses of micro-instability using parameters referring to HL-2A plasma by means of GKNET. In Sec. 3.1, at first, we study the micro-instability in HL-2A plasma without and with ECRH. We found a new type of drift instability. For studying the origin of the instability, we investigate different temperature and density profile are shown to study in Sec. 3.2. The effect of Λ_e is studied to understand the role of ECRH onset for ion-ITB collapse in Sec. 3.3. In all the simulations, the equilibrium radial electric field is not taken in to account for simplicity.

3.1 Linear analysis based on HL-2A plasma parameter

Table 1 shows the main parameters at 400 ms (before ECRH) and 500 ms (after ECRH) in shot 22388 of HL-2A experiment [1], which magnetic field strength is $B_0 = 1.31$ T and safety factor profile is $q(r) = 1.02 - 3.22(r/\alpha)^2 + 6.93(r/\alpha)^3$. After ECRH is applied, we can see that electron temperature gradient becomes steep, while ion temperature gradient is flat due to profile relaxation.

Table 1 Main parameters in shot 22388 of HL-2A experiment.

	R_0/L_{T_i}	R_0/L_{T_e}	R_0/L_n	η_i	η_e	a/R_0
400 ms	13.61	12.62	10.48	1.31	1.20	0.24
500 ms	8.98	13.88	9.09	0.99	1.52	0.24

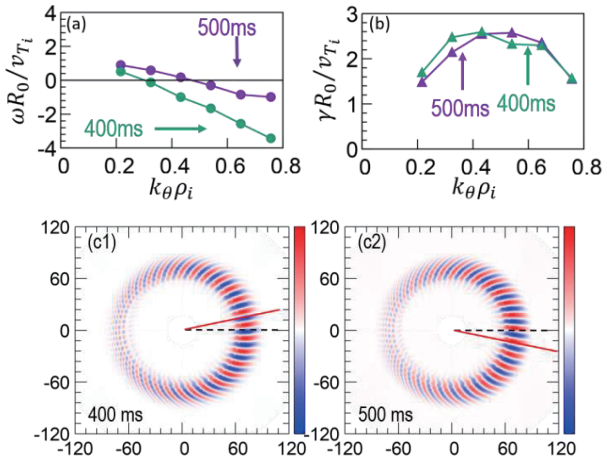

Fig. 1 (a) Real frequency over $k_\theta\rho_i$ and (b) linear growth rate as a function of poloidal wavenumber $k_\theta\rho_i$. The corresponding electrostatic potential structures with $k_\theta\rho_i = 0.44$ are shown in (c1) and (c2). Note that we zoom up the structure by focucing $0 < r < 120$.

Based on the above two sets of parameters, we perform linear toroidal gyrokinetic simulations. Figures 1 (a) and (b) show the real frequency and growth rate with respect to $k_\theta\rho_i = nq\rho_{ti}/r$ estimated at $r = a/2$, so that $k_\theta\rho_i$ is simply proportional to the toroidal mode number n. It is found that the real frequency changes from positive to negative value continuously at both 400 ms and 500 ms. This feature is different from the standard ITG mode and TEM characterized by negative and positive real frequency following the direction of ion and electron diamagnetic drift over the whole region of $k_\theta\rho_i$ in our model.

It is found that, before ECRH, the maximum growth rate is $\gamma R_0/v_{Ti} \sim 2.6$ at $k_\theta\rho_i \sim 0.42$ and the corresponding real frequency is $\omega R_0/v_{Ti} \sim -1.0$, while after ECRH, $\gamma R_0/v_{Ti} \sim 2.6$ at $k_\theta\rho_i \sim 0.52$, and $\omega R_0/v_{Ti} \sim -0.31$, so that the real frequency shifts to a low frequency relatively near to zero and $k_\theta\rho_i$ which provides the maximum growth rate shifts to a high value. Figures 1 (c1) and (c2) show the electrostatic potential structures at 400 ms and 500 ms, respectively. It is found that they show nearly up-down symmetry on the poloidal cross section in both cases, which tilting angles from the mid-plane are nearly zero [5].

3.2 Parameter scans for temperature and density gradients

In order to study the nature of the mode with low fre-

Table 2 Main parameters for parameter scan.

Parameter	R_0/L_{T_i}	R_0/L_{T_e}	R_0/L_n	η_i	η_e
A	15.5	4.0	2.1	7.4	1.9
B	4.0	15.5	2.1	1.9	7.4
C1	4.0	4.0	2.1	1.90	1.90
C2	4.0	4.0	7.4	0.54	0.54
C3	4.0	4.0	11.5	0.35	0.35
C4	4.0	4.0	15.5	0.26	0.26

quency shown in Fig. 1, here we perform parameter scans for R_0/L_{Ti}, R_0/L_{Te} and R_0/L_n. The parameter sets are listed in Table 2. Case A has a steep ion temperature gradient ($R/L_{Ti} = 15.5$) and a flat electron temperature gradient ($R/L_{T_e} = 4.0$). Contrary to case A, case B has a steep electron temperature gradient ($R/L_{T_e} = 15.5$) and a flat ion temperature gradient ($R/L_{T_i} = 4.0$). Note that flat density gradient ($R/L_n = 2.1$) is set in both case A and B. On the other hand, in cases C1-C4, we change the density gradient ($R/L_n = 2.1, 7.4, 11.5, 15.5$), while keeping same relatively flat ion and electron temperature gradients ($R/L_{T_i} = R/L_{T_e} = 4.0$). In these scans, we use a safety factor profile in Cyclone Base Case [6] described by the function $q(r) = 0.85 + 2.18(r/\alpha)^2$.

Figure 2 shows (a) real frequency and (b) linear growth rate as a function of $k_\theta\rho_i$ in case A, B and C2. In case A, we can see the characteristics of the standard ITG mode that the real frequency is negative and the linear growth rate has a local maximum at $k_\theta\rho_i \sim 0.5$. In case B, the real frequency is positive and the growth rate is shifted to the high-$k_\theta\rho_i$ region, which corresponds to the standard TEM. In Case C1, we observe no unstable mode. On the other hand, in case C2 which has a steeper density gradient, modes with lower frequency across zero are found to appear, which is similar to those seen in the simulation using HL2A parameters in Fig. 1. Figures 2 (c1), (c2) and (c3) show electrostatic potential structures corresponding to case A, B and C2, respectively. We can see that the titli ng angle is positive in case A (ITG mode) while negative in case B (TEM), which results from the different signs of th e real frequency of ITG mode and TEM in a global toroidal geometry.

Figure 3 shows (a) real frequency and (b) linear growth rate in case C2-C4. From Fig. 3 (a), we can see that the absolute values of real frequency increase with density gradient as well as the growth rate where the maximum value shifts to the high-$k_\theta\rho_i$ region. These modes are considered to be induced mainly by the steep density gradient with small η_i and η_e, which is a different tendency from that of the standard ITG mode and TEM.

According to Ref. [7], there exists a different kind of TEM. It is driven by the density gradient with the essential role of trapped electrons, which is called as the density gradient driven TEM (ε_n-TEM). Interestingly, the real frequency of ε_n-TEM is low and often goes across zero. This

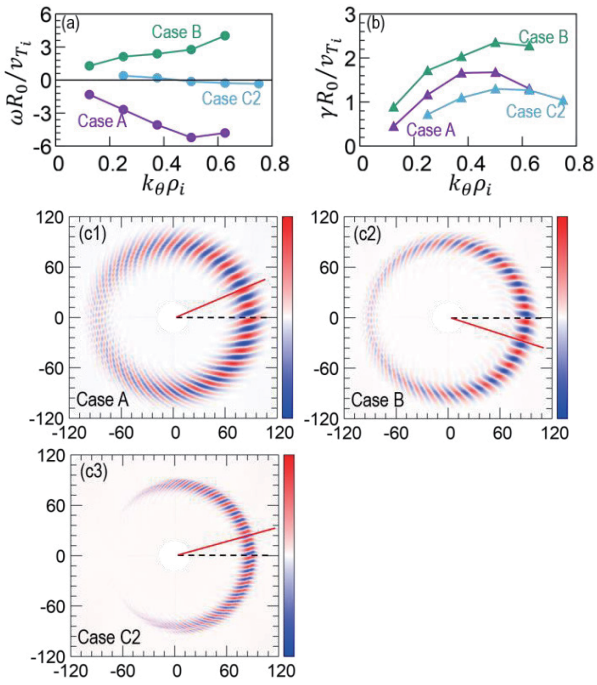

Fig. 2 (a) Real frequency and (b) linear growth rate as a function of the poloidal wavenumber $k_\theta\rho_i$ for case A, B and C2. The corresponding electrostatic potential structures are shown in (c1) - (c3).

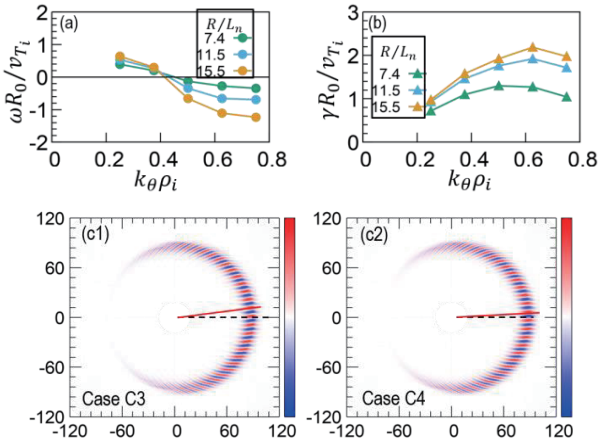

Fig. 3 (a) Real frequency and (b) linear growth rate as a function of $k_\theta\rho_i$ for case C2-C4. Corresponding R_0/L_n are 7.4, 11.5, 15.5. The electrostatic potential structures of case C3, C4 is shown in (c1-c2) with $k_\theta\rho_i = 0.6$.

characteristic is similar to the present mode observed in the present case C2-C4.

3.3 Effect of ECRH

In Sec. 3.2, it is found that the density gradient is the main driving force for the present mode with low frequency which is considered to appear in the HL-2A experiment. Since ITB collapses after ECRH onset, in this subsection, we simulate the effect of ECRH on such mode by changing the ratio $\Lambda_e = T_{e\perp}/T_{e\|}$ from 0.5 to 2.0.

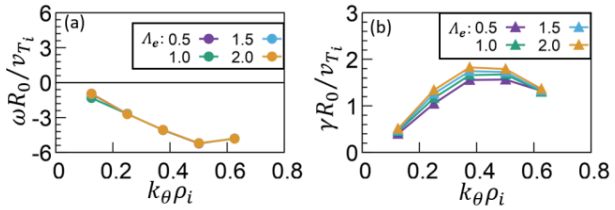

Fig. 4 (a) Real frequency and (b) linear growth rate over $k_\theta\rho_i$ with different Λ_e for standard ITG mode (case A).

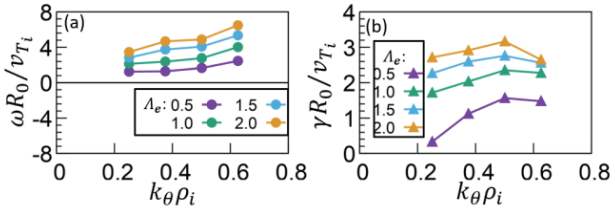

Fig. 5 (a) Real frequency and (b) linear growth rate over $k_\theta\rho_i$ with different Λ_e for standard TEM (case B).

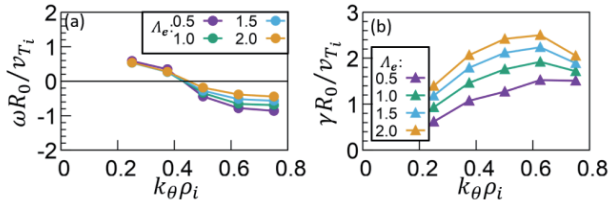

Fig. 6 (a) Real frequency and (b) linear growth rate over $k_\theta\rho_i$ with different Λ_e for the intermediate mode (case C3).

Figures 4 and 5 show the effect of Λ_e on the standard ITG (case A) and standard TEM (case B), respectively. From Fig. 4 (a), we can see that the real frequency of ITG mode is almost independent on $T_{e\perp}$. A weak dependence of growth rate on $T_{e\perp}$ can be observed in Fig. 4 (b) and the growth rate linearly rises by about 15% from $\Lambda_e = 0.5$ to $\Lambda_e = 2$. When both ion and electron temperature profiles are steep but with a flat density profile as case C1, such a case shows the same feature as shown in Fig. 4.

On the other hand, unlike the standard ITG mode, the standard TEM shows a strong sensitivity on $T_{e\perp}$ as shown in Fig. 5. Both real frequency and growth rate of the TEM increase with $T_{e\perp}$. The growth rate is increased to 2.14 times from $\Lambda_e = 0.5$ to $\Lambda_e = 2$. As mentioned in Sec. 2, the fraction of trapped electron becomes larger by increasing $T_{e\perp}$. In addition, larger Λ_e leads to increase electron precession drift velocity, which usually makes TEM unstable [8].

Figure 6 shows the effect of Λ_e on the present mode with low frequency (case C3). From Fig. 6 (a), it is found that the real frequency has little dependence on $T_{e\perp}$ like the standard ITG mode, but the growth rate shows a different tendency. Here it should be noted that there are two interesting features. The first, the growth rate is much smaller than that of the ITG mode or TEM but increased to 1.80 times from $\Lambda_e = 0.5$ to $\Lambda_e = 2$. Therefore, we conclude that the mode with low frequency can be destabilized by the increase of $T_{e\perp}$ realized by ECRH. The second, the growth rate spectrum tends to have a peak value at $k_\theta\rho_i \sim 0.6$ as shown in Fig. 6 (b), which is similar to the standard ITG mode.

4. Conclusion

In this work, we studied micro-instabilities using parameters in the HL2A plasma with ion-ITBs based on the GKNET simulations which include kinetic electron dynamics in a global toroidal geometry. Specifically, we found a new type of drift mode which is expected to appear in the HL-2A plasma with peaked density together with relatively flat ion and electron temperature profiles. The mode is destabilized by trapped electrons as TEM while exhibits different features as found from the study changing the ratio $\Lambda_e = T_{e\perp}/T_{e\parallel}$. The main characteristics are summarized as follows;

(1) the real frequency is close to zero and change the sign from electron diamagnetic direction to that of ion with the increase of $k_\theta\rho_i$, which is weakly dependent on $T_{e\perp}$ like ITG mode, (2) the growth rate is increased with larger density gradient, which is different from that of the standard ITG mode and TEM, (3) the growth rate is also sensitive to $T_{e\perp}$ similar to TEM. Thus, the mode is found to exhibit low frequency and/or hybrid characteristics between ITG mode and TEM.

We will perform more detailed analysis on the mode with low frequency driven by the density gradient by changing other parameters such as aspect ratio and safety factor and compare the results with the local dispersion analyses [7]. Nonlinear simulation is also requested to understand the role of the mode on the transport in a future work.

Acknowledgments

The authors would like to gratefully acknowledge Dr. D. L. Yu and Dr. J. Y. Kim for helpful discussions. This work was supported by JSPS KAKENHI Grant 17H01180, 16K17844 and also partially supported by the Natural Foundation of China under Grant No.11775069.

[1] D.L. Yu *et al.*, Nucl. Fusion **56**, 056033 (2016).
[2] K. Imadera *et al.*, Proc. 26th Int. Conf. on Fusion Energy, TH/P3-3 (2016).
[3] K. Imadera *et al.*, Proc. 25th Int. Conf. on Fusion Energy, TH/P5-8 (2014).
[4] A.J. Brizard and T.S. Hahm, Rev. Mod. Phys. **79**, 421 (2007).
[5] Y. Kishimoto *et al.*, Plasma Phys. Control. Fusion **41**, A663 (1999).
[6] A.M. Dimits *et al.*, Phys. Plasmas **7**, 969 (2000).
[7] J.Y. Kim and H.S. Han, Phys. Plasmas **24**, 072501 (2017).
[8] T.S. Hahm, Phys. Fluids B **3**, 1445 (1991).